Thermally activated depinning motion of contact lines in pseudopartial wetting

Lingguo Du, Hugues Bodiguel,* and Annie Colin
Univ. Bordeaux, CNRS, Solvay, LOF UMR 5258, France
(Received 16 April 2014; published 9 July 2014)

We investigate pressure-driven motion of liquid-liquid menisci in circular tubes, for systems in pseudopartial wetting conditions. The originality of this type of wetting lies in the coexistence of a macroscopic contact angle with a wetting liquid film covering the solid surface. Focusing on small capillary numbers, we report observations of an apparent contact angle hysteresis at first sight similar to the standard partial wetting case. However, this apparent hysteresis exhibits original features. We observe very long transient regimes before steady state, up to several hundreds of seconds. Furthermore, in steady state, the velocities are nonzero, meaning that the contact line is not strongly pinned to the surface defects, but are very small. The velocity of the contact line tends to vanish near the equilibrium contact angle. These observations are consistent with the thermally activated depinning theory that has been proposed to describe partial wetting systems on disordered substrates and suggest that a single physical mechanism controls both the hysteresis (or the pinning) and the motion of the contact line. The proposed analysis leads to the conclusion that the depinning activated energy is lower with pseudopartial wetting systems than with partial wetting ones, allowing the direct observation of the thermally activated motion of the contact line.

DOI: 10.1103/PhysRevE.90.012402 PACS number(s): 68.08.Bc, 68.35.Ja

I. INTRODUCTION

Contact line dynamics has been the focus of a long-lived debate for several decades (see for a recent review Ref. [1]). The difficulties arise because of the many length scales involved: experiments usually focus on macroscopic properties, the contact angle, whereas its static and dynamic properties are governed by microscopic details at the three-phase contact point. It is worthwhile mentioning that wetting dynamics is involved in many scientific and technological areas, for example, in the coating industry or in biphasic flows in porous media. Two major types of wetting are usually encountered, depending on the sign of the spreading coefficient. The latter is defined as the energy difference between a nonwetted solid surface and a wetted one, i.e., by $S = \gamma_s - \gamma_{sw} - \gamma_{wn}$, where γ_s, γ_{sw}, and γ_{wn} are the surface energies of the solid surface, the solid phase-wetting phase interface, and the wetting phase-nonwetting phase interface, respectively. When S is negative, a nonzero contact angle is a solution of Young's law, whereas when S is positive, a wetting film covers the whole surface at equilibrium. Such a macroscopic description is, however, incomplete, since when considering the details of interaction forces, another type of wetting is encountered depending on the shape of the disjoining pressure [2]. When the interaction forces between the solid surface and the fluid interface are repulsive at short distances and attractive at longer ones, there is a wetting film covering the surface similarly to complete wetting situations, but this film coexists with a macroscopic nonzero contact angle θ_e, similarly to the partial wetting case. This situation has been referred to as *pseudopartial wetting* and has stimulated several theoretical work [2–5]. A rather limited number of observations has been reported [6–12], but we recently argued and showed that when considering liquid-liquid-solid systems, pseudopartial wetting is much more frequent [13]. The aim of this paper is to focus on the contact line dynamics of this type of wetting.

Two main classes of models have been proposed to describe contact line motion. The first and more popular one is based on hydrodynamic considerations. Viscous dissipation in the liquid wedge is responsible for an increase, respectively decrease, of the dynamic contact angle θ_d for an advancing, respectively decreasing, contact line [14–16]. Many experimental facts are well accounted for by these hydrodynamic approaches (see for a review Ref. [17]). The other class of models are based on Eyring's activated rate theory [18] and derived from Blake's early idea that the motion of the contact line is thermally activated at the microscopic scale [19]. These molecular kinetic theories (MKT) have been extended further [20,21] and tested on various systems, but available experimental data may not be sufficient to discriminate between the two approaches [22].

However, both these descriptions do not describe the contact angle hysteresis [23], which is systematically present with partial wetting systems. The contact line is pinning and immobile whenever the contact angle θ is greater than a receding contact angle θ_r and lower than an advancing contact angle θ_a. The presence of this hysteresis has been attributed to the presence of surface defects [16,24–27], which can be of either chemical or topographic nature. Recent experimental evidence has shown that a single defect as small as a few nanometers leads to a hysteresis of the contact line motion [28], which underlines that contact angle hysteresis is a general feature of the dynamics of partial wetting systems. In fact, although the contact angle hysteresis could be reduced to a few degrees with ultra-clean and atomically smooth surfaces, it is usually much higher. Any wetting dynamics problem needs to face this issue, which is highly important at low capillary numbers ($\mathrm{Ca} = \eta V/\gamma$, where η is the viscosity, V the contact line velocity, and γ the surface tension), since the above mentioned theories predict that the dynamic contact angle reaches a constant value for $\mathrm{Ca} < 10^{-4}$.

Another approach has been proposed by Prevost *et al.* [29] and leads to a description that unifies the contact angle hysteresis and the contact line motion when viscous

*hugues.bodiguel@u-bordeaux.fr

dissipation could be neglected [30]. The physical idea is that the motion of the contact line is governed by thermally activated local jumps between pinning sites on a disordered surface, under a force $f = \gamma(\cos\theta_e - \cos\theta_d)$ per unit of length. The related model is also derived from Eyring's theory and is thus similar to MKT; i.e., the velocity is proportional to $\exp(-E^*/k_BT)\sinh\left(f\lambda^2/k_BT\right)$, where λ is the activation length, k_B the Boltzmann constant, T the temperature, and E^* an activation energy. However, the physical signification of the activation length and activation energy is different since they correspond to depinning events, whereas it is related to molecular adsorption in MKT. One of the important consequences is that this model accounts for the contact angle hysteresis [30] and predicts that a very slow thermally activated motion should exist between the advancing and receding contact angles.

This model has been validated on a rather limited number of systems. The thermally activated motion has been nicely demonstrated by Prevost *et al.* taking advantage of vicinity of the wetting transition of helium on disordered cesium substrate [29], and tested further with liquid nitrogen [30]. Remarkably the sizes of the depinning jumps were found to be on the same order as the size of the substrate defects, i.e., 10 nm. More recently, various liquids were tested on gold surfaces [31], but without such a clear relation between the activation length and the substrate topography. It is worthwhile mentioning that other groups reported high values of the activation length using a thermally activated fit to their data, as, for example, in the case of a water-dodecane system on hydrophobic substrates [32–34], which clearly indicates the relevance of the thermally activated depinning motion. Again, the motion at low velocities was found to be related to the disorder of the substrate [34]. All these studies show that the transition from pinning to depinning is not sharp and thermally activated. However, the depinning activation energy is rather high, leading to a strong pinning between advancing and receding of the contact line.

In this article, we aim at describing the motion of the apparent contact line of pseudopartial wetting systems. This offers an opportunity to test the above models of contact line motion, as the presence of a wetting film covering the surface should affect the dynamics. In a recent publication, we reported that these systems exhibit an apparent contact angle hysteresis, without any macroscopic pinning [13]. Here we first report that steady state is hardly achieved in these systems in the vicinity of the equilibrium contact angle and analyze the transient regimes observed before steady state. Then we focus on the steady-state velocity of the meniscus and analyze it within the framework of the thermally activated depinning theory.

II. MATERIALS AND METHODS

A. Systems

Several solid-liquid-liquid systems are used to get various wetting situations, and are listed in Table I. They consist in dodecane and an aqueous solution or a fluorinated oil (FC-40), in glass tubes grafted either with octadecyltrichlorosilane (OTS) or 1H,1H,2H,2H-perfluorooctyl-trichlorosilane (PFTS). For each system, the interfacial tension γ is determined using the pendant drop method. The spreading coefficient S is defined by $S = \gamma_{sw} - \gamma_{so} - \gamma$, where γ_{so} and γ_{sw} are the surface tensions of the oil-solid interface and of the aqueous solution-solid interface, respectively, and determined using contact angle measurements of a drop of oil on the solid surface in air and a drop of water in the same conditions. A simple combination of Young's law then allows deducing the value of S. The sign of S distinguishes partial wetting systems ($S < 0$) from complete or pseudopartial wetting ($S > 0$). Except for the glass-PFTS surface, all the systems exhibit a positive spreading coefficient, meaning that there is in principle a film of oil covering the surface. This is confirmed experimentally when trying to deposit a droplet of the nonwetting fluid on a planar solid surface immersed in the wetting fluid. The droplet stands on the surface and freely rolls on it when the surface is slightly tilted.

TABLE I. Measured interfacial tension and spreading parameter S at 25 °C of the systems used. CTAB stands for an aqueous solution of cetyltrimethylammoniumbromide at 2×10^{-6} g/L. FC-40 is a fluorinated oil with the molecular formula $C_{21}F_{48}N_2$. The viscosities of the liquids are 0.89 mPa s (all aqueous solutions), 3.4 mPa s (FC-40) and 1.34 mPa s (dodecane).

Systems	γ (N/m)	S (N/m)
Partial wetting		
Glass-PFTS/dodecane/water	43.2×10^{-3}	-2.9×10^{-3}
Pseudopartial wetting		
Glass-OTS/dodecane/water	43.2×10^{-3}	2.4×10^{-3}
Glass-OTS/dodecane/CTAB	35.7×10^{-3}	11.9×10^{-3}
Glass-OTS/dodecane/FC-40	5.1×10^{-3}	11×10^{-3}

When the spreading coefficient is positive, the equilibrium contact angle could be either zero for complete wetting systems or nonzero for pseudopartial wetting systems. In order to discriminate between the two possibilities, we deposit a drop of the wetting liquid on the same surface immersed in the nonwetting phase. In all the three systems listed as "pseudopartial" in Table I, a droplet remains stable at long times with a finite contact angle. The fact that these systems are in a pseudopartial situation could be explained by contributions of the silane layer (see Ref. [13] for further details) to the surface interactions. Without this layer, the systems are in partial wetting. Correlatively, and limiting ourselves to the Van Der Waals contribution, the interaction between water and glass is attractive; i.e., the Hamaker constant of the glass-dodecane-water system is positive [13]. For oil films much thicker than the one of the silane layer, the contribution to the disjoining pressure of this layer could be neglected as the interactions with the semi-infinite glass wall dominate. Therefore, the interaction between the solid-wetting fluid interface and the wetting-nonwetting fluid switches from repulsive to attractive when increasing the thickness of the wetting fluid layer. This leads to pseudopartial wetting, consistent with the above-mentioned observations.

B. Experimental setup and methods

In order to investigate the dynamics of liquid-liquid-solid contact lines, we study the displacement of a single meniscus in a circular tube under an imposed pressure drop.

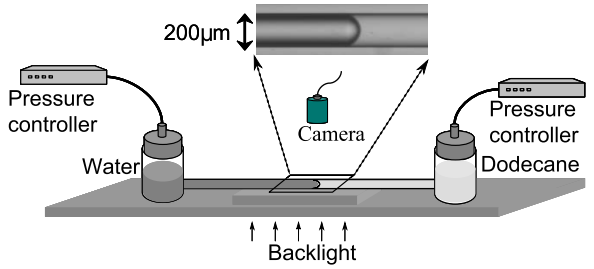

FIG. 1. (Color online) Schematic drawing of the experimental setup. The picture is an advancing meniscus in a glass-PFTS-dodecane-water system.

The experimental setup, sketched in Fig. 1, consists in two reservoirs connected by a horizontal circular glass tube of radius $R = 100\,\mu$m and length $L = 8$ cm, commercialized by VitroCom (supplied by CTS) and silanized by OTS. The capillary tube is suspended in midair by drilling two holes about 1 cm high from the bottom of the two reservoirs, which are glass vials of 30 ml. The tube extends several millimeters in the interior of the two vials and are bonded by an epoxy adhesive. The main objective of this setup is to ensure that a single meniscus is formed between the two reservoirs.

The reservoir containing the wetting fluid is first filled, leading simultaneously to the filling of the tube. Then the other reservoir is filled with the nonwetting fluid. Both vials are connected to a pressure controller (Fluigent MFCS), which allows one to impose pressures, with an accuracy of about 6 Pa. By applying a pressure on the nonwetting fluid reservoir, a single meniscus is created in the tube. We adjust the pressure so that it lies approximately in the middle of the tube. Its displacement is recorded using a camera (AVT Pike 505B) mounted on an Olympus SZX16 binocular. A precise image analysis software allows us to measure the meniscus relative displacement with a precision of about 200 nm. The liquid heights in the reservoir are adjusted to equalize the hydrostatic pressure difference. Given the high volumes of the reservoir as compared to that of the tube, the meniscus displacement in the tube corresponds to a negligible variation of the reservoir height. The precision of the height measurement is about 1 mm, so that the uncertainty on the hydrostatic pressure difference is below 10 Pa.

As will be detailed in the next section, a steady state is not reached immediately for pseudopartial wetting systems. Transient regimes as long as hundreds of seconds are observed depending on the applied pressure drop. It is thus necessary to respect a strict protocol in order to obtain reproducible results. In particular, every change of the applied pressure drop needs to be followed by a long waiting time in order to be able to reach a steady state and thus to erase memory of previous pressure variations. We have systematically used the following protocol. Starting with a meniscus a few centimeter away from the observation field, a first pressure drop ΔP_i is applied. When the meniscus enters the observation field (usually more than 10 min after), a sudden change of pressure drop from ΔP_i to ΔP is made, and the meniscus displacement is monitored.

III. RESULTS

Let us first focus on the meniscus velocity measured just after a sudden change of the pressure drop, for the pseudopartial wetting systems. Starting from a steady state under a pressure drop ΔP_i, a step in pressure from ΔP_i to ΔP is applied at $t = 0$. Figure 2 displays some examples of the measured meniscus position z as a function of time. Despite the pressure controller setting the pressure in much less than 1 s, the meniscus displacement exhibits a transient regime during which the unsigned velocity decreases asymptotically towards constant value. This effect can occur for both advancing and receding menisci. The time scale of this transient regime is highly dependent on the pressure drop ΔP, since it can hold as long as several tens of seconds, as in Fig. 2(a), but can also be too short to be observable, as in Fig. 2(b). We even occasionally observed durations of the transient regimes of several thousands of seconds, but these situations were hard to reproduce, meaning that the characteristic time can be very sensitive to the experimental conditions.

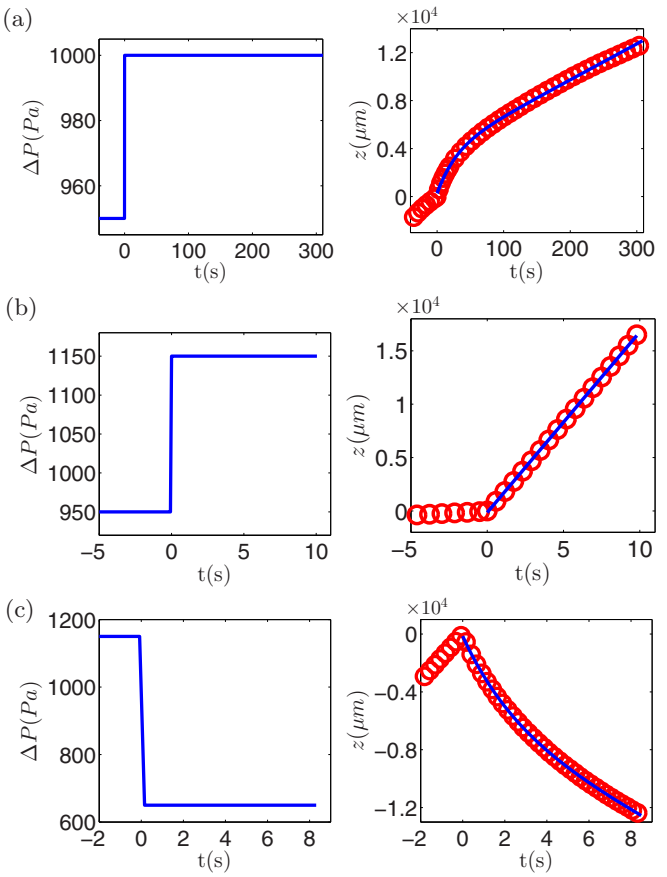

FIG. 2. (Color online) Examples of menisci positions measured after a step in the imposed pressure drop for the glass-OTS-dodecane-water system. For each example, the left axes displays the pressure drop as a function of time, and the right axes the corresponding meniscus position. The experimental meniscus position data (red circles) are fitted (blue solid lines) with Eq. (1). The fitted parameter for these three cases are (a) $\tau = 0.1 \pm 0.05$ s, $v_\infty = 1708 \pm 50\,\mu$m/s, (b) $\tau = 28.1 \pm 0.5$ s, $v_\infty = 30.1 \pm 0.4\,\mu$m/s, and (c) $\tau = 2.5 \pm 0.5$ s, $v_\infty = -754 \pm 50\,\mu$m/s.

Since the data are consistent with an exponential relaxation for the meniscus velocity, we systematically fit the meniscus

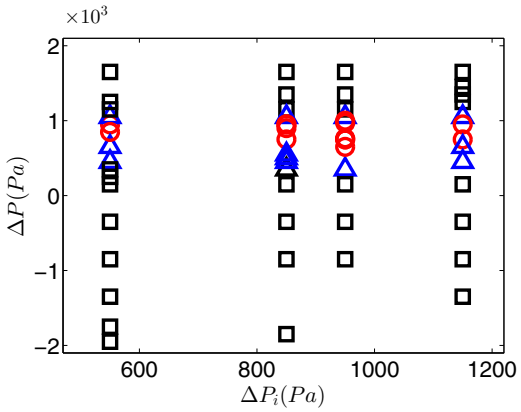

FIG. 3. (Color online) Diagram showing the couples $(\Delta P_i, \Delta P)$ that have been investigated for the system glass-OTS-dodecane-water. The symbol shapes indicate the order of magnitude of the transient regime. Squares correspond to experiments where the steady state is reached almost instantaneously (lower than 2 s), triangles to experiments where $2 < \tau < 500$ s, and circles when $\tau > 500$ s.

position z with the following relation:

$$z - z_0 = A \exp\left(-\frac{t}{\tau}\right) + v_\infty t, \tag{1}$$

where z_0 is the meniscus position at $t = 0$, v_∞ is the asymptotic meniscus velocity, and τ a characteristic time. As shown in Fig. 2, this empirical model well describes the experimental data.

We first test the dependence of the duration of the transient regime on the two pressure drop ΔP_i and ΔP, i.e., the pressure drops imposed before and during the transient regime. Figure 3 represents the amplitude of the value of the characteristic time τ in this space parameter. Long transient regimes clearly occur in a domain where, for the glass-OTS-dodecane-water system, ΔP lies between 500 and 1000 Pa, independently of the pressure drop ΔP_i. This means that the characteristic time does not depend on the pressure history. Accordingly, we have checked that the asymptotic meniscus velocity v_∞ is also independent on ΔP_i, so that we refer to it in the following as the steady-state velocity.

Figure 4 displays the characteristic time τ and the steady-state meniscus velocity v_∞ as a function of the pressure drop ΔP.

The meniscus velocity displays at first sight three regimes: at low and high values of ΔP, the velocity increases linearly with the pressure drop. In between, the velocities are rather small, typically below 1 μm/s, and an apparent plateau is observed. It is important to note that, though very small, the meniscus velocity never vanishes in this regime (see the semilog plot in insert of Fig. 4); the contact line is not pinned. This is in contrast with partial wetting systems, where a contact line hysteresis is observed, leading to a regime at first sight similar but with vanishing velocities due to contact line pinning. In a previous communication [13], we already report this observation with various systems and referred to as an apparent contact angle hysteresis.

The variations of the characteristic time τ with the pressure displayed in Fig. 4, evidence a correlation with the

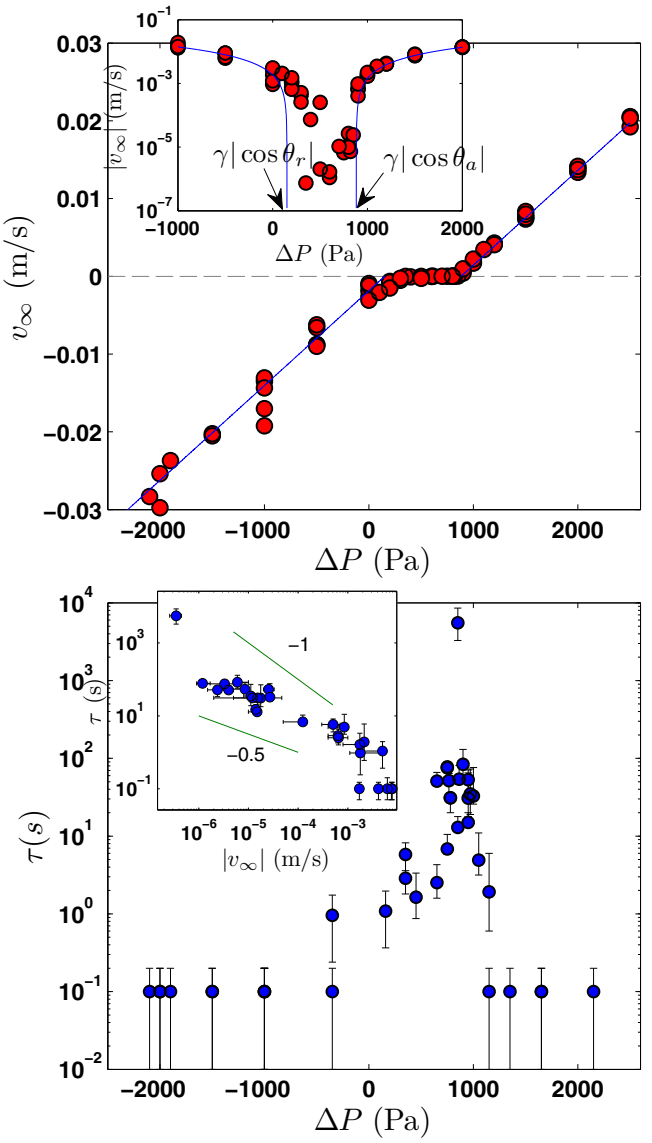

FIG. 4. (Color online) Top: Steady-state velocity v_∞ for the glass-OTS-water-dodecane system as a function of the imposed pressure drop. The solid lines are the best linear fit to the data in the upper and lower viscous branches. The slope is 1.22×10^{-5} m/s/Pa. Their intersections with the zero-velocity line defines an apparent receding pressure drop of $-\gamma \cos\theta_r = 151$ Pa and an apparent advancing pressure drop of $-\gamma \cos\theta_a = 882$ Pa. In between these pressure drops and as shown in the insert (same data), the velocity does not vanish but is very small. Bottom: Characteristic time τ of the transient regime for the same system. The insert displays the empiric correlation of the characteristic time with respect to the absolute value of the steady-state velocity. The solid lines correspond to a power law of exponent -1 and -0.5. When no transient regimes are observed, τ is arbitrarily set to 0.1 s.

steady-state velocity. The long transient regimes coincide with the apparent hysteresis region. In the two linear branches, values of τ are very small. The correlation between τ and v_∞ is illustrated in insert of Fig. 4. For both advancing and receding menisci, the characteristic time falls on a single monotonically decreasing curve when plotted as a function of the unsigned steady-state velocity. The smallest steady-state velocity, the

highest relation time. Although the scatter in the data does not allow us to state concerning a robust scaling, the global trend might be captured using a power law, $\tau \propto v_\infty^n$, with an exponent lying between -0.5 and -1. If one forces it to -1, then a length scale appears from this empiric scaling and is on the order of 1 mm.

The results presented above have been obtained using the pseudopartial wetting system glass-OTS-dodecane-water. Similar transient regimes also occur with the other pseudopartial wetting systems (see Table I). In contrast, we have never observed such regimes with partial wetting or complete wetting systems. Therefore, it seems that the transient regimes reported here are, similarly to the apparent hysteresis [13], a particular feature of pseudopartial wetting.

IV. DISCUSSION

A. Steady-state velocity

As detailed in the previous section and in Ref. [13], all the pseudopartial wetting systems we have studied exhibit a similar behavior in steady state. The meniscus velocity exhibits three regimes as a function of the pressure drop. In both the low- and high-pressure regimes, the velocity increases linearly as a function of the pressure drop, and in the intermediate regime, the velocity is much smaller but the contact line is not pinned. Since the length of the tube is about 1000 times the tube radius, the additional dissipation in the meniscus region could be safely neglected together with end effects, and the Poiseuille law applies upstream and downstream from the meniscus. By summing the upstream, downstream, and Laplace pressure contributions, the total pressure drop should verify

$$\Delta P = -2\frac{\gamma \cos\theta_d}{R} + \frac{8vL}{R^2}[\eta_1 z + \eta_2(1-z)], \qquad (2)$$

where η_1 and η_2 are the liquid viscosities, $\tilde{z}$ is the relative meniscus position in the tube, and v the meniscus velocity, corresponding to the mean flow velocity. The dynamic contact angle θ_d is defined in the nonwetting phase.

Using thereafter nondimensional quantities defined by $\tilde{P} = \Delta P R/2\gamma$ and $\tilde{V} = 4\bar{\eta}vL/\gamma R$, where $\bar{\eta} = (\eta_1 + \eta_2)/2$, the previous equation reduces to

$$\tilde{P} = -\cos\theta_d + \tilde{V}\frac{\eta_1\tilde{z} + \eta_2(1-\tilde{z})}{\bar{\eta}} = -\cos\theta_d + a\tilde{V}. \qquad (3)$$

Since $\tilde{z}$ is set around 0.5 and does not vary significantly during the experiments, and since the fluid viscosities are on the same order of magnitude, a is close to unity. From Eq. (3), one could directly interpret the two linear branches of the $\Delta P - V$ experimental relations. They correspond to a fixed dynamic contact angle. These have been experimentally verified and reported in Ref. [13]. As recalled in the introduction, the dynamic contact angle is known to increase for advancing menisci and to decrease for receding ones. This effect is well accounted for by hydrodynamic theories such as the Cox-Voinov law [15]. It becomes significant for capillary numbers $\eta v/\gamma$ greater than 10^{-3}. In our experiments, the capillary number never exceeds this value, so that we expect constant dynamic contact angles, consistent with our measurements in the low and pressure drop regimes. In the intermediate regime, the dynamic contact angle varies, but this is not due to viscous forces.

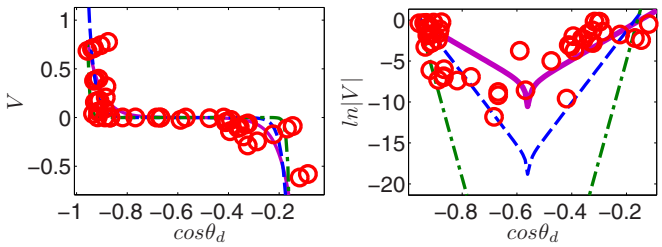

FIG. 5. (Color online) Normalized meniscus velocity as a function of $\cos\theta_d$ for the OTS-dodecane-water (pseudopartial wetting). Experimental data (circles) are displayed in linear (left) and log scale (right). The three lines correspond to the thermally activated depinning model [Eq. (4)] with three couples of parameters λ and E^*: 2 nm, 31 k_BT (solid line), 3 nm, 43 k_BT (dashed line), and 5 nm, 72 k_BT (dashed dotted line). We decide that the values of λ around 3 nm and E^* around 43 k_BT describe best the data.

We use Eq. (3) to extract the dynamic contact angle. To do so, we first measure the empiric value of the constant a, which is simply the slope of the two linear branches at high and low pressure drops. The constant a remains close to unity, but due to some uncertainties, its value is typically between 0.9 and 1.1. Knowing this value, the dynamic contact angle is deduced from Eq. (3). Figure 5 displays the resulting plot of the meniscus velocity as a function of the dynamic contact angles, for the glass-OTS-water-dodecane system. The data exhibit two asymptotic dynamic contact angles for advancing and receding velocities, separated by a region where the contact angle varies significantly, recalling the contact angle hysteresis commonly observed with partial wetting systems. Contrary to standard contact angle hysteresis, the contact line is not pinned but exhibits a small velocity as shown in the log axes in Fig. 5. This velocity is positive for $\cos\theta_d < -0.55$ and negative otherwise.

Such a variation of the contact angle with very small velocities has been reported for partial wetting systems but with very low viscosities [29,30]. To describe these experiments, the authors proposed a thermally activated depinning theory. The idea is that the contact line jumps from one pinning site to another, due to thermal energy. Neglecting hydrodynamic forces, this model leads to the following prediction for the contact line velocity [29,30]:

$$v = \lambda\nu_0 \exp\left(-\frac{E^*}{k_BT}\right)\sinh\left[\frac{\lambda^2\gamma}{k_BT}(\cos\theta_e - \cos\theta_d)\right], \qquad (4)$$

where ν_0 is the thermal frequency (k_B/h), E^* the activation energy, θ_e the equilibrium contact angle, and λ the typical size of the contact line jumps. Although it has been argued that the E^* and λ could depend on the sense of the contact line motion [30], we were not able to detect a clear symmetry difference between advancing and receding menisci. Thus, we choose in the following to use the same values for receding and advancing menisci.

Given the rather important scatter in the experimental data at very low velocities, we did not try to fit them directly using Eq. (4). This choice is also motivated by the huge variations of the sinh function in the range of velocities measured. Three unknown parameters appear in Eq. (4): E^*, λ, and $\cos\theta_e$. It is

intrinsically not possible to know the value of θ_e for pseudopartial wetting systems from independent measurements without the knowledge of the disjoining pressure. Since our data show a rather good symmetry from the middle of the two asymptotic values of the dynamic contact angle (see Fig. 4), we set the equilibrium contact angle at this value. We are left with two fitting parameters, but these are highly constrained by the two asymptotic values of the dynamic contact angle in the high-velocity branches. For a given value of the jump length λ, we first determine the activation energy E^* that describes the range of the apparent hysteresis. Indeed, as pointed out by Rolley and Guthmann [30], the contact angle hysteresis verifies $\cos\theta_r - \cos\theta_a \simeq E^*/\lambda^2$. Then we manually choose the best (E^*,λ) couple that accounts for the order of magnitude of the velocity in the apparent hysteresis region. This is achieved graphically. As shown in the log plot in Fig. 5, a small variation of the jump length λ leads to huge variations of the meniscus velocity. Therefore, though far to be accurate, this procedure enable us to find the appropriate model parameter that describes the observations in a robust way. For the glass-OTS-water-dodecane system displayed in Fig. 5, we find typical values of $\lambda = 3$ nm and $E^* = 43\,k_BT$ for this system.

Although the scatter in the data prevents us from a convincing verification of Eq. (4), the latter accounts reasonably well for the low velocities measured inside the apparent contact angle hysteresis.

We have used this procedure for the different pseudopartial wetting systems and for the partial wetting one. All the pseudopartial wetting systems exhibit a very similar behavior, i.e., an apparent contact angle hysteresis without pinning. The partial wetting system is rather different. There is a clear pressure drop range where the contact line is pinned, between the two linear viscous branches. Even when waiting a few hours, no meniscus displacement could be observed. This is depicted in Fig. 6 where we arbitrary set the velocities of the pinned menisci at very low values. The fact that there are pinned or unpinned menisci for a given $\cos\theta_d$ value probably originates from different locations in the tube. In order to account for the observation of pinned contact lines, the only possibility is to set the E^* parameters at a value that is greater

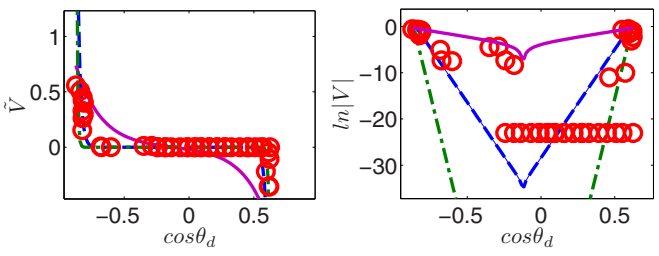

FIG. 6. (Color online) Normalized meniscus velocity as a function of $\cos\theta_d$ for the PFTS-dodecane-water (partial wetting). The lines correspond to the thermally activated depinning model [Eq. (4)] with three couples of parameters λ and E^*: 1 nm, 26 k_BT (solid line), 3 nm, 57 k_BT (dashed line), and 5 nm, 120 k_BT (dashed dotted line). In order to capture the zero velocities, we decide to choose values of λ larger than 5 nm and E^* equals 120 k_BT. The zero velocities are arbitrary set as $V = 10^{-10}$ m/s in the log-scale axis.

TABLE II. Estimated parameters of the thermally activated depinning model for the various partial and pseudopartial wetting systems studied.

Systems	θ_e (°)	λ (nm)	$E^*/(k_BT)$
Partial	97	5	120 (>120)
Water	124	3	43 (35, 50)
CTAB	150	3	35 (30, 45)
FC-40	165	20	43 (38, 50)

than 120 k_BT. Lower values would lead to velocities that we would have detected experimentally. Note that the value of 120 k_BT falls in the range of the previously reported one, which is 100–1000 k_BT [1].

Table II summarizes the parameter values for the three pseudopartial and for the partial wetting system. There is a striking difference between the two sets of systems concerning the order of magnitude of the activation energy. It is much higher for the partial wetting system than for the pseudopartial ones. Let us recall that this activation energy is the argument of an exponential factor so that the consequences of this difference are huge. In usual conditions with partial wetting systems, the thermally activated motion of the contact line is not observed. The contact line is strongly pinned by the surface defect until the departure from equilibrium reaches a high value. The transition from a strong pinning to a moving contact line is sharp, and once it starts to move, viscous dissipation controls the dynamics. This behavior matches the classical picture of contact angle hysteresis.

For pseudopartial wetting, the important decrease of the activation energy might be understood as due to the wetting film, which smoothes the defects of the surface. The local jumps from one pinning site to another are much more frequent than without this wetting film. Pseudopartial systems thus offer in usual experimental conditions the opportunity to observe the thermally activated motion of the contact line, "inside" the contact angle hysteresis.

The values of the jump length λ are not easy to understand without a good knowledge of the surface. Unfortunately it is rather hard to perform some measurements inside the tube, such as atomic force microscopy. Furthermore, we do not think we can use flat surfaces as references, as it is not possible to perform the exact grafting procedure used in tube. The values of λ reported in Table II are, however, on the order of a few nanometers, which seems quite reasonable for a silanized glass surface. The high value of λ measured for the FC-40 system is larger, although it was obtained with the same surface. Note that the difference with the other systems is quite important. It has been recently argued and shown that this length is not simply related to the surface characteristic distances and could vary on the same surface from one system to another [31]. Clearly future experiments will need to be conducted on surfaces having well-defined properties to be able to go further with the interpretation of the jump sizes.

B. Transient regimes

Let us now come back to the observation of long transient regimes. As shown in Fig. 4 the long transient regimes we

reported seem to be closely linked to the apparent contact angle hysteresis since characteristic times are long only in this regime. When the steady-state velocity is below 1 mm/s, characteristic times are greater than a few seconds and increase significantly (up to hundreds of seconds) when the absolute value of the steady-state velocity decreases. According to the thermally activated depinning theory, the velocity is related to the departure from equilibrium. Thus, it seems that the closer to equilibrium, the higher the relaxation time.

From an experimental point of view, the existence of a very long transient regime requires a precise protocol. In order to measure the steady-state velocity, it is necessary to wait a great amount of time. This is why we have used for the experiments in steady state such a precise protocol. If the pressure is changed during the transient regime, then meniscus displacement is very hard to understand, and reproducibility is difficult to ensure. It seems that the meniscus movement is then governed by the history of the pressure variations. The slow motion observed in the apparent hysteresis regime is observed only with a fixed pressure drop. If the pressure drop is fluctuating, then the meniscus velocities remain higher than a few hundreds of micrometer per seconds. We could also extrapolate that the menisci velocities will remain at high values in situations where the geometry is more complex than in a tube of constant radius.

Similar transient regimes have also been observed occasionally in other systems. With a water-cyclohexane system, Chertcoff *et al.* have studied the meniscus dynamics in a millimeter-size glass capillary tube initially saturated with cyclohexane, which is water wet [35]. Their setup is very similar to the one we have used, since the meniscus movement is controlled by a pressure difference. After a sudden change of pressure, they report transient regimes of characteristic time that could be as high as a few hundreds of seconds. These effects are particularly strong at very low capillary numbers between 3×10^{-9} and 5×10^{-7}. It seems that these observations are very similar to ours, but unfortunately the authors do not specify the exact type of wetting of their system. Given the fact that we have only seen these kinds of transient regimes in pseudopartial wetting conditions, it is attractive to think that the systems they used are also in pseudopartial wetting conditions. The authors suggest that the relaxation is due to adsorption sites with a wide range of characteristic times: decreasing the velocity increases the number of sites active for adsorption and enhances the wetting of a high-energy glass surface by water. However, such an interpretation does not really explain why there exists long transient regimes at very low capillary numbers. Their theoretical description remains an open issue.

V. CONCLUSION

We have studied the dynamics of a liquid-liquid meniscus in a circular tube at small capillary numbers in pseudopartial wetting conditions. With this particular class of wetting systems, there exists a wetting film covering the solid surface which coexists with a macroscopic contact angle. The results reported here highlight the unusual properties of the wetting dynamics of these systems. Compared to partial wetting and complete wetting, two main differences are observed. In between an advancing contact angle and a receding one, the meniscus velocity in steady state is very slow but never vanishes, in contrast with partial wetting systems which exhibit contact angle hysteresis with a strong pinning of the contact line. In this regime, steady state is, however, hard to reach since transient regimes involving higher velocities are surprisingly as long as hundreds of seconds. None of these two observations could be accounted for by standard viscous dissipation either in the bulk or in the liquid wedge close to the contact line.

We propose here an interpretation of the apparent contact angle hysteresis that is based on the thermally activated depinning motion of the contact line. In this theory, initially proposed by Prevost and Rolley [29], a strong dissipation arises from contact line fluctuations close to the equilibrium contact angle and leads to slow velocities. In partial wetting systems such as the one reported in the literature together with the one reported here, activation energy corresponding to local jumps of the contact line to one pinning site to another is greater than $100\, k_B T$, which implies that the pinning is strong, in agreement with standard contact angle hysteresis. With pseudopartial wetting systems, we find that the activation energy is much lower, from 30 to 50 $k_B T$. Such a value allows an observable contact line motion inside the contact angle hysteresis, at room temperature. Although more precise measurements are needed to be able to claim a clear agreement with the model which contains two fitting parameters, the experimental results reported here are rather well described by this approach. It is not clear yet if this framework could be compatible with the observation of long transient regimes. A time-dependent out-of-equilibrium thermodynamic theory seems to be needed.

Future work should deal with better defined solid surfaces in order to be able to link the thermally activated depinning motion to the substrate topography.

[1] D. Bonn, J. Eggers, J. Indekeu, J. Meunier, and E. Rolley, Rev. Mod. Phys. **81**, 739 (2009).

[2] F. Brochardwyart, J. M. Dimeglio, D. Quere, and P. G. Degennes, Langmuir **7**, 335 (1991).

[3] H. Wong, S. Morris, and C. J. Radke, J. Colloid Interface Sci. **148**, 317 (1992).

[4] E. K. Yeh, J. Newman, and C. J. Radke, Colloids Surf., A **156**, 525 (1999).

[5] K. D. Humfeld and S. Garoff, Langmuir **20**, 9223 (2004).

[6] K. Ragil, J. Meunier, D. Broseta, J. O. Indekeu, and D. Bonn, Phys. Rev. Lett. **77**, 1532 (1996).

[7] L. Esibov, D. Sarkisov, U. S. Jeng, M. L. Crow, and A. Steyerl, Physica B **241–243**, 1077 (1997).

[8] H. Kellay, J. Meunier, and B. P. Binks, Phys. Rev. Lett. **69**, 1220 (1992).

[9] H. Matsubara, T. Shigeta, Y. Takata, N. Ikeda, H. Sakamoto, T. Takiue, and A. Aratono, Colloids Surf. A **301**, 141 (2007).

[10] K. M. Wilkinson, C. D. Bain, H. Matsubara, and M. Aratono, ChemPhysChem **6**, 547 (2005).
[11] V. Bergeron and D. Langevin, Phys. Rev. Lett. **76**, 3152 (1996).
[12] Y. Cheng, X. Ye, X. D. Huang, and H. R. Ma, J. Chem. Phys. **125**, 164709 (2006).
[13] L. Du, H. Bodiguel, C. Cottin, and A. Colin, Chem. Eng. Proc. **68**, 3 (2013).
[14] O. V. Voinov, Fluid Dyn. **11**, 714 (1977).
[15] R. G. Cox, J. Fluid Mech. **168**, 169 (1986).
[16] P. G. de Gennes, Rev. Mod. Phys. **57**, 827 (1985).
[17] J. H. Snoeijer and B. Andreotti, Annu. Rev. Fluid Mech. **45**, 269 (2013).
[18] R. Eyring, *The Theory of Rate Processes* (McGraw-Hill, New York, 1941).
[19] T. D. Blake and J. M. Haynes, J. Colloid Interface Sci. **30**, 421 (1969).
[20] T. D. Blake, M. Bracke, and Y. D. Shikhmurzaev, Phys. Fluids **11**, 1995 (1999).
[21] D. Duvivier, D. Seveno, R. Rioboo, T. Blake, and J. D. Coninck, Langmuir **27**, 13015 (2011).
[22] D. Seveno, N. Dinter, and J. D. Coninck, Langmuir **26**, 14642 (2010).
[23] T. D. Blake, J. Coll. Inter. Sci. **299**, 1 (2006).
[24] J. F. Joanny and P. G. Degennes, J. Chem. Phys. **81**, 552 (1984).
[25] M. O. Robbins and J. F. Joanny, Europhys. Lett. **3**, 729 (1987).
[26] A. Paterson, M. Fermigier, P. Jenffer, and L. Limat, Phys. Rev. E **51**, 1291 (1995).
[27] S. Moulinet, A. Rosso, W. Krauth, and E. Rolley, Phys. Rev. E **69**, 035103(R) (2004).
[28] M. Delmas, M. Monthioux, and T. Ondarçuhu, Phys. Rev. Lett. **106**, 136102 (2011).
[29] A. Prevost, E. Rolley, and C. Guthmann, Phys. Rev. Lett. **83**, 348 (1999).
[30] E. Rolley and C. Guthmann, Phys. Rev. Lett. **98**, 166105 (2007).
[31] K. Davitt, M. S. Pettersen, and E. Rolley, Langmuir **29**, 6884 (2013).
[32] R. Fetzer, M. Ramiasa, and J. Ralston, Langmuir **25**, 8069 (2009).
[33] R. Fetzer and J. Ralston, J. Phys. Chem. C **114**, 12675 (2010).
[34] M. Ramiasa, J. Ralston, R. Fetzer, and R. Sedev, J. Phys. Chem. C **116**, 10934 (2012).
[35] R. Chertcoff, A. Calvo, I. Paterson, M. Rosen, and J. P. Hulin, J. Colloid Interface Sci. **154**, 194 (1992).